Mine Water and the Environment (2021) 40:308–319
https://doi.org/10.1007/s10230-020-00746-y

TECHNICAL ARTICLE

Identification of Flow Zones Inside and at the Base of a Uranium Mine Tailings Dam Using Geophysics

Erika Juliana Aldana Arcila[1] · César Augusto Moreira[1] · Pedro Lemos Camarero[2] · Matheus Felipe Stanfoca Casagrande[1]

Received: 26 February 2020 / Accepted: 4 December 2020 / Published online: 5 January 2021

Abstract
Potential problems related to a tailings dam's stability are a matter of concern, especially where structural failure might endanger nearby communities and the environment. The Osamu Utsumi mine, located in the State of Minas Gerais, is currently not operating. The rock-soil tailings dam has water upwelling downstream in the bedrock, with water flux confined to rock fractures. This research was conducted to identify possible flux zones in the base of the dam using DC resistivity and electrical resistivity tomography (ERT). The data acquisition consisted of five ERT lines with 6 m of spacing between electrodes, using a Schlumberger array. The results are presented by 2D and 3D geophysical models comprising measured and processed resistivity values. It was possible to identify a low resistivity zone (5–20 Ωm), whose structural continuity indicates water infiltration in the bedrock under the dam. Moreover, the results do not indicate that erosion is taking place in the interior of the dam, reducing the risk of geotechnical instability and failure of physical integrity.

Keywords Mining · 3D model · DC resistivity · ERT

Introduction

A tailings dam is a barrier, whose function is the accumulation of residual products from mining and ore processing. The design methods for tailings dams differ from water retention dams by their construction in different stages, but the stability of both are very important. This is especially true for dams built for the storage of mining waste, since failures threaten the safety of people, industrial property, and the environment (Mainali 2006). An infamous example is the tailings dam rupture that occurred in 1985 near Tesero (Trento), in northern Italy. The tailings dam in the Stava valley (Italy) failed due to internal erosion problems, killing 268 people (Chandler et al. 1995; Sammarco 2004).

More recently, there was two major tailings dam failures (in 2015 and 2019), that affected the municipalities of Mariana and Brumadinho in the state of Minas Gerais, in southeast Brazil. These events spilled millions of cubic meters of iron tailings and destroyed areas of native vegetation, contaminated water bodies, and killed more than 200 people (IBAMA 2019). Given these events, the Federal Government has increased supervision of mining companies to ensure constant maintenance and monitoring of tailings dams, to comply with Brazil's environmental legislation, which through Law No. 12.334 (2010), established the National Dam Safety Policy, with the aim of maintaining structural and operational integrity, preservation of life, health, property and the environment (IBAMA 2017).

However, for many companies, the cost of monitoring dams with conventional geotechnical techniques can be relatively high. Lower-cost alternatives, such as geophysical methods,

✉ Pedro Lemos Camarero
camarero@folha.com.br

Erika Juliana Aldana Arcila
julianaaldana.a@gmail.com

César Augusto Moreira
moreirac@rc.unesp.br

Matheus Felipe Stanfoca Casagrande
casagrande@hotmail.com

[1] Geosciences and Exact Sciences Institute (IGCE), Universidade Estadual Paulista (UNESP), 24-A Avenue, 1515, Bela Vista, Rio Claro, São Paulo State 13506-900, Brazil

[2] Science and Technology Institute (ICT), Universidade Federal de Alfenas (UNIFAL), José Aurélio Vilela Highway, 11999, Cidade Universitária, Poços de Caldas, Poços de Caldas, Minas Gerais State 37715- 400, Brazil

are being increasingly used to complement traditional geotechnical techniques. These alternatives are non-invasive, low-cost tools that are widely used to investigate geological structures (Camarero et al. 2019). In addition, they can be used to establish contrasts between surface material and the rocky substrate, or artificial fill and natural land. Therefore, they can be used to monitor, control, and understand the phenomena that influence problems arising from the existence of these dams (Kearey et al. 2002; Mussett and Khan 2000).

Many of the accidents that occur in dams are associated with problems of water infiltration, such as seepage and internal erosion of the soil. Internal erosion may be caused by the construction of dams on permeable soils or dispersive clays, the use of inappropriate or defective materials, excessive rainfall, the presence of animals that live or take refuge in the soil, such as rodents that form galleries in the edaphic environment. Water flow inside a dam favors the development of underground ducts that can cause the material layer to collapse and accelerate the erosion process (Lewis 2014; Oliveira and Brito 1998). Depending on the physical parameter to be measured, the methods to control and monitor these can be direct, such as monitoring of wells and piezometers, or indirect, such as geophysical (gravimetric, seismic, magnetic, electrical, and radioactive methods), which can be used to obtain information on hydrogeological and structural aspects, lithological changes in the materials and other relationships between the material and water (Al-Fares 2014; Mussett and Khan 2000).

Case studies of dams inspected by geophysical methods have been reported (Al-Fares 2014; Asfahani et al. 2010; Assumpção et al. 2002; Bedrosian et al. 2012; Bièvre et al. 2017; Camarero et al. 2019; Coulibaly et al. 2017; Lghoul et al. 2012; Lin et al. 2013, 2018; Minsley et al. 2011; Oh and Sun 2007; Osazuwa and Chinedu 2008; Sjödahl et al. 2005; Zarroca et al. 2014); and there are reports of case studies to improve storage capacity of tailing dams (Ozcan et al. 2013; Wei et al. 2016).

The INB company requested a geotechnical study to ascertain the physical integrity of of a rock and earth dam built for the accumulation of uranium mine tailings. The geophysical survey of the dam was carried out using electric resistivity tomography (ERT) to identify areas of water flow and possible underground channels formed by infiltration inside the dam and the rock massif. The objective was to diagnose any risk of geotechnical instability or loss of the dam's physical integrity.

The Study Area

The study area is located in the State of Minas Gerais, southeastern Brazil, on the Poços de Caldas plateau. This region belongs to the municipality of Caldas, 30 km from the cities of Poços de Caldas, Andradas, and Águas da Prata. The plateau has a nearly circular area, measuring about 800 km^2, 30 km in diameter, with an altitude of 500 m above the surrounding regions (Fig. 1).

Approximately 30 km southwest of Caldas is the Indústrias Nucleares do Brasil (INB) company's Osamu Utsumi mine and its mining treatment unit (MTU). This MTU occupies an area of nearly 18 km^2 and was built to contain tailings from the currently inactive mining and processing of uranium (World Nuclear Association 2020).

The deposit is a product of hydrothermal and supergene processes, comprising a sequence of volcanic and subvolcanic phonolites and nepheline syenite intrusions associated with volcanic breccia pipes (Waber et al. 1992). The MTU of Poços de Caldas was deactivated in 1995 and decontamination of its facilities began in 2005 (Franklin 2007). The operation process was divided into three areas. The first was the mineral extraction area (the Osamu Utsumi open pit uranium mine), which is nearly circular and has a diameter of 1200 m, with a maximum depth of 200 m (Fig. 2—area A). The second area was the physical and chemical beneficiation area, where the ore was subjected to primary and secondary crushing, grinding, and thickening to reduce the particle size of the mineral to 800 µm and obtain a neutral pulp suitable for transport to the processing plant. Subsequently, the mineral pulp was subjected to a chemical process that involved leaching, vacuum filtration, clarification, and in the final stage, mixing and decanting processes to produce a uranium concentrate in the form of ammonium diurate—DUA (yellow cake), from which the fuel element for nuclear reactors is obtained (Fig. 2—area B). The last area was the tailings dam, in which the low uranium mineral pulp was released for particle decantation and the water was reused for the ore processing (Fig. 2—area C) (Franklin 2007).

The Tailings Dam

The tailings containment system consists of an earth and rock dam, which is situated at the Soberbo river valley, adjacent to the Antas river basin, separated by a topography, which constitutes the natural watershed of the place.

The dam's function was to create a reservoir to deposit liquid waste from the industrial beneficiation process. Effluent waters, from rainfall and infiltration, are treated downstream of the dam before the wáter is returned to the natural water course.

The dam's slope has a curved axis with a radius of 380 m, is NE–SW oriented, and is 435 m in length, with its concavity downstream, and its top is 1310 m high. The body of the structure consists of highly compacted rock fill, measuring up to 42 m at its central axis, and containing 1.97×10^6 m^3 of tailings. The dam has an upwardly inclined clay core,

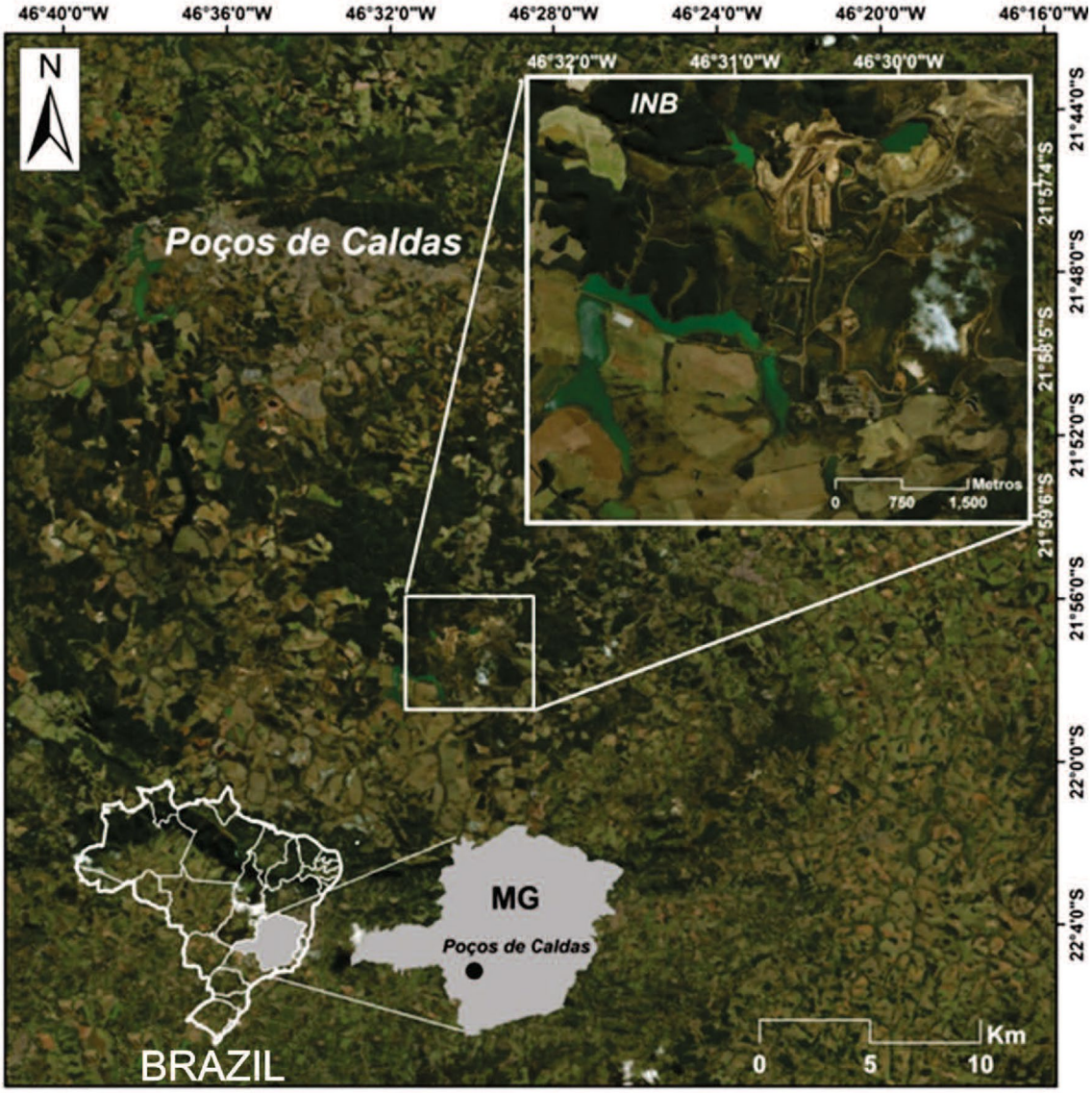

Fig. 1 Location of the INB—Poços de Caldas (MG)

with two levels of construction visible downstream, and is monitored by a series of piezometers (Fig. 3). The dam has chimney sub-vertical sand filters between the clay core and the upstream and downstream rocks. The transition filter system is connected to a horizontal drainage mat to capture the filtered water in the dam body and in the bedrock-supported foundations. The bedrock follows the topography of the local relief, so it tends to be closer to the surface near the abutments.

The spillway is a tulip-shaped structure, connected to a concrete gallery, that rests on the right shoulder of the dam, both in the sub-horizontal section (below the dam massif) and in the sub-vertical section. It is supported by the slope and following the original topography. The water flows freely through concrete pipes. All water downstream is collected in storage pools and fed to a deflector system, where the effluent is treated with barium chloride solution ($BaCl_2$) to reduce its radium (Ra) concentration.

On the surface, near the central axis downstream of the dam, an area of upwelling can be seen. This flow occurs in a fractured system oriented orthogonally to the dam's axis. The most important fracture in the outcrop has a N40W/38SW orientation. This condition may indicate water flow under the dam that crosses the dam/solid rock contact. The local lithology is composed of phonolites—potassic igneous rock.

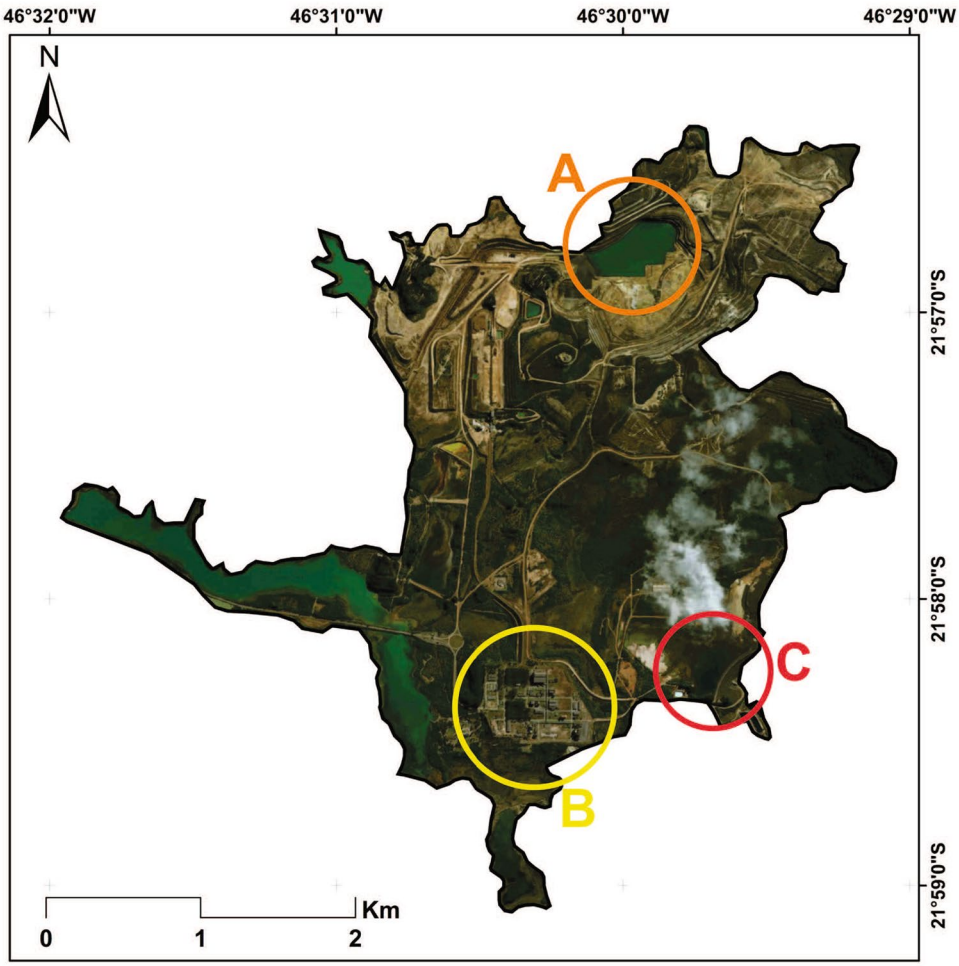

Fig. 2 Mining treatment unit (MTU): **a** Poços de Caldas Osamu Utsumi uranium open pit; **b** physical–chemical processing area; **c** tailings dam (study area)

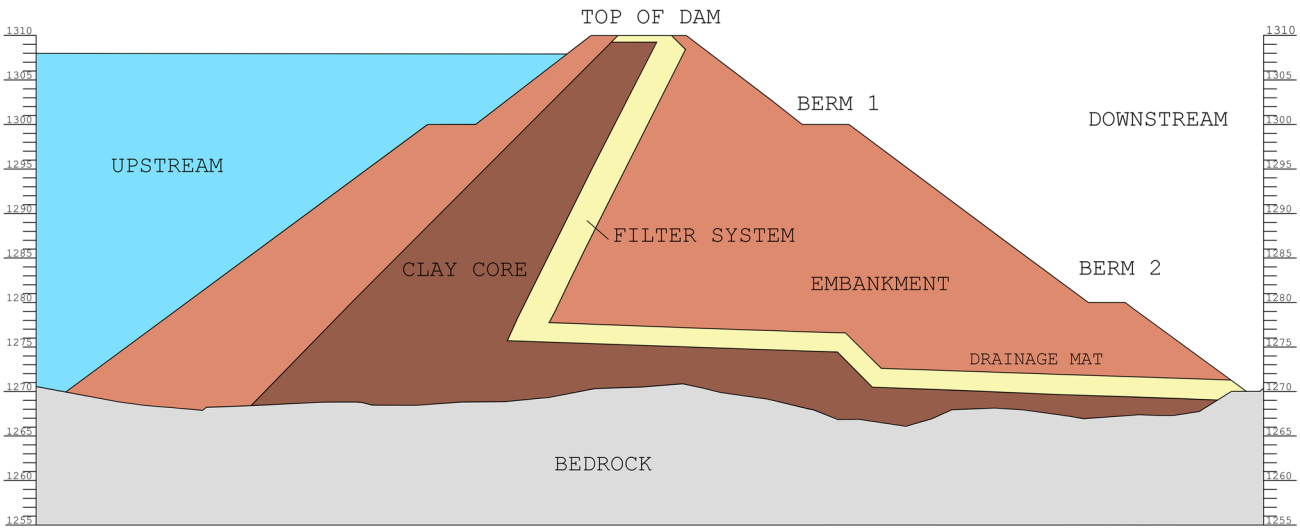

Fig. 3 Dam design profile

Materials and Methods

Geophysical methods can be used to develop a subsurface geology model, locate fracture zones, investigate groundwater systems and contamination plumes, and obtain information about the physical and lithological parameters of the soil (Knödel et al. 2007). Electrical resistivity (ER) is a geoelectric method, which uses alternating or direct low frequency current (0.1–30 Hz) to investigate the electrical properties (resistivity) of the subsurface and thus detect fractures and cavities, and delineate the soil's hydrogeological characteristics (Mussett and Khan 2000; Thompson et al. 2012; Sentenac et al. 2018; Albuquerque et al. 2019).

In this way, ER data were obtained for the INB tailings dam by means of five lines of electrical resistivity tomography (ERT). Lines 1, 2, and 3 were arranged on the crest of the dam (left side, center, and right side) and lines 4 and 5 were made on the berms of the slope (Fig. 4a).

Note that the dam is 42 m high at its central point. Lines 1 and 3 were located close to the dam's embankment, where the original relief of the valley contacts the dam's abutment and the rock massif is variable, and less than 42 m in height. The gap between electrodes was 6 m, based on the estimated dimensions of the body and the desired depth of investigation; the lines were oriented in the SW direction towards the NE. These lines intercept the massif major geologic fracture, where it was possible to identify water upwelling (Fig. 4b).

Lines 1 and 3 were 114 m in length, with 20 electrodes each, while line 2 was 156 m in length with 27 electrodes. Lines 4 and 5 each measured 240 m in length and had 41 electrodes, placed in parallel and 14 m apart from each other, corresponding to the vertical length between berms, which allowed complete coverage of the dam's entire length.

The dam has a curved axis; however, straight lines were arranged for the field measurements to avoid alterations in depth. As for the effects of the topography, there were some variations in the length of the lines, specifically on the abutments.

The equipment used was the ABEM Terrameter LS resistivity meter, produced in Sweden (ABEM 2012). The instrument allowed us to perform ER tests, and automatically calculate contact resistance and standard deviation of the measurement set through the Schlumberger array. This technique is recommended for vertical electrical sounding (VES) investigations which is considered the best technique for rock structures when the objective is to observe resistivity variations with depth (Lowrie 2007).

The resistivity data was processed using RES2DINV inversion software. This program automatically subdivides the subsoil into several blocks and then uses a statistical model based on the least squares method to determine the appropriate resistivity value for each block. The software determines the error criterion, then the inverted resistivity model is modified to reduce the degree of error between the measured and calculated apparent resistivity. This operation

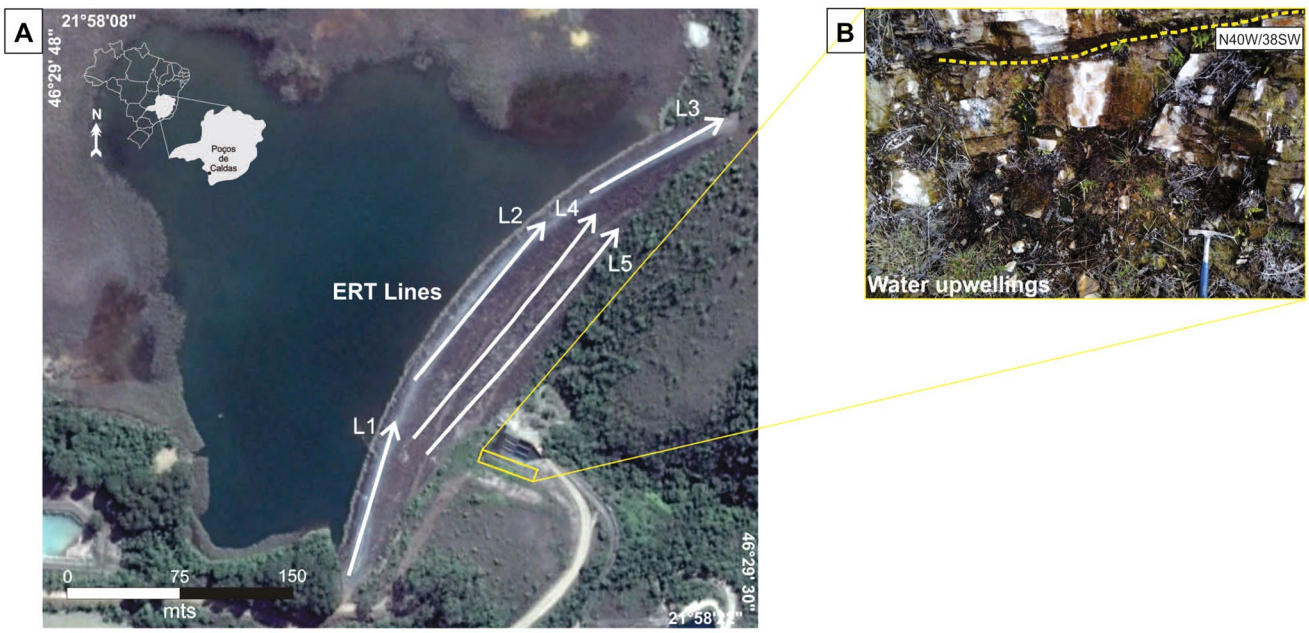

Fig. 4 **a** Arrangement of geophysical lines in the study area; **b** water upwellings at the rock massif in the dam's foundation

is repeated iteratively until the error reaches an aceptable value (Coulibaly et al. 2017; Moreira et al. 2017).

For geological structures, a three dimentional (3D) resistivity study that uses a 3D interpretative model provides the most accurate results. The 3D data set consists of several parallel rows in two dimentional (2D). The models of each 2D line were exported individually in xyz format through RES2DINV to provide 2D cross sections. Finally, the entire data set was combined into a 3D data set and imported using Oasis Montaj Geosoft software (version 6.4) to obtain 3D visualization models. The visualization models of this work were created by applying the minimum curvature algorithm and the files were imported to the same software (Moreira et al. 2017; Lin et al. 2013; Loke 2000).

The data acquisition software must be able to take into account the electrode configuration, electrode spacing, and other survey parameters. For 3D resistivity models, multichannel instruments are essential to reduce data acquisition time to an acceptable level (Loke 2000).

Results and Discussion

In 2D electrical tomography inversion models and 3D block models, resistivity values are expressed in Ωm through a chromatic, logarithmic scale to analyze the variation of resistivity values. The lowest values, between 5 and 20 Ωm (cold colors), represent low resistivity or wet areas and high values, between 300 and 600 Ωm (warm colors), represent the most resistive values or dry areas.

The models showed high resistivity patterns in the upper sections (Fig. 5). Lines 1, 2, and 3 show a thicker upper resistive horizon with values between 300 and 600 Ωm. In the deeper sections, the resistivity decreases considerably with the lowest resistivity values (5 Ωm) downstream and laterally, as indicated in the highlighted areas. The blue colored areas in lines 1, 2, and 3 represent the most significant water flow zones; one can observe the continuity of water flow laterally from an elevation of 1290 m, from line 1 to line 2 and from line 2 to line 3.

Line 4 has a superior area characterized by high resistivity, although it is thinner than lines 1, 2, and 3. From ≈ 15 m deep, it shows a low resistivity area and a zone between 45 and 60 m with less than 20 Ωm of resistivity associated with the presence of water; however, it does not show the significant resistivities associated with large volumes of water flow. Line 5 shows greater lateral variations of low resistivity, with two 20 Ωm areas between 9 and 30 m and 84 and 90 m.

However, all of the profiles had a region with resistivities between 39 and 300 Ωm, between the elevation of 1310 and 1280 m, which could be related to the construction materials of the dam, such as the compacted clay core and the transition system (sand and gravel) connected to the drain mat, which are less resistive materials. In all of the profiles, the high resistivity values observed in the upper coverage of the images are associated with the type of rock or rockfill.

The resistivity decreases as the depth increases in the 2D electric tomography inversion models, with significant deviations on the sides of the dam. Considering the geometry of the dam and the relief of the valley, it is likely that some of these are water pathways in the massif - mainly in low resistivity zones on lines 4 and 5 and in some areas of lines 1 and 3. The infiltration that occurs in line 2 is directly associated with flow lines and the positioning of the dam drainage system.

Lines 1, 2, and 3 were at the top of the dam, upgradient of the filter system, while lines 4 and 5 were downgradient of the filter system. In line 5, there are two infiltration zones. The first is round and located at the 1270 m level; it is interpreted as a wet zone resulting from the drainage mat, since it occurs at the contact between the dam's embankment and the massif. The second, on the upper left, is interpreted as an infiltration area in the massif, due to its depth of occurrence and the dam's geometry; this zone is also identifiable on line 4.

The ERTs of the 2D lines were joined to produce the 3D model. Initially, a 3D block model was generated with a front, back, and base view of the dam (Fig. 6). With these 3D interpolation models, it is possible to more clearly identify the areas with water flow.

In the frontal view (Fig. 6a), it is possible to observe high resistivity areas (300–600 Ωm) in the upper sections that belong to the rockfill, following the design of the structure. The areas of low resistivity (between 15 and 35 Ωm) on the sides stand out; these indicates the prevalence of water-saturated rock at the ends of the dam. The raised points represent the lowest resistivities (5–9 Ωm) or wet regions. On the left side, there is a significant volume of water compared to the right side. However, the rear view (Fig. 6b) clearly shows two points of low resistivity in the middle portion associated with water flow from 1290 m in elevation. The views of the front and rear base (Fig. 6c and d) suggest that this flow occurs from NW to SE, as indicated by the arrows.

Note that the largest volume of water flows inside the rock massif below the dam and on its left side, and a rocky basement occurs at an elevation of 1290 m (30 m deep) on the sides of the dam. These facts are extremely important for the research, considering that the infiltration occurs on the same side of the fractured massif that presents the water upwellings (Fig. 4b).

In the same set of images, another significant resistivity zone between 70 and 20 Ωm was identified, on the right side of the dam (Fig. 6a). Although it does not point to the presence and continuity of water flow in the upper sections, it is possible to identify a less resistive zone on the dam's surface

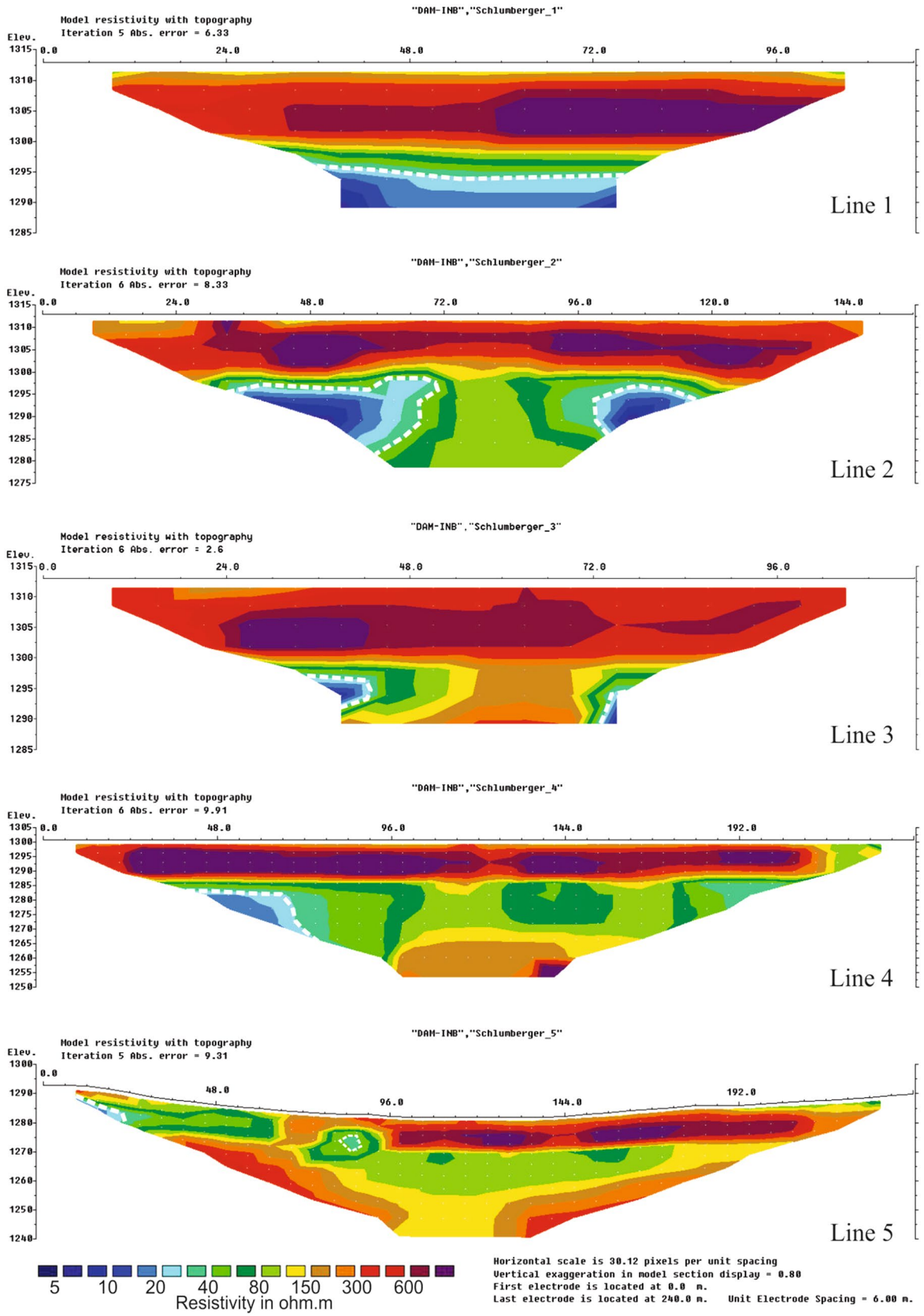

Fig. 5 The ERTs inversion with highlight in low resistivity areas

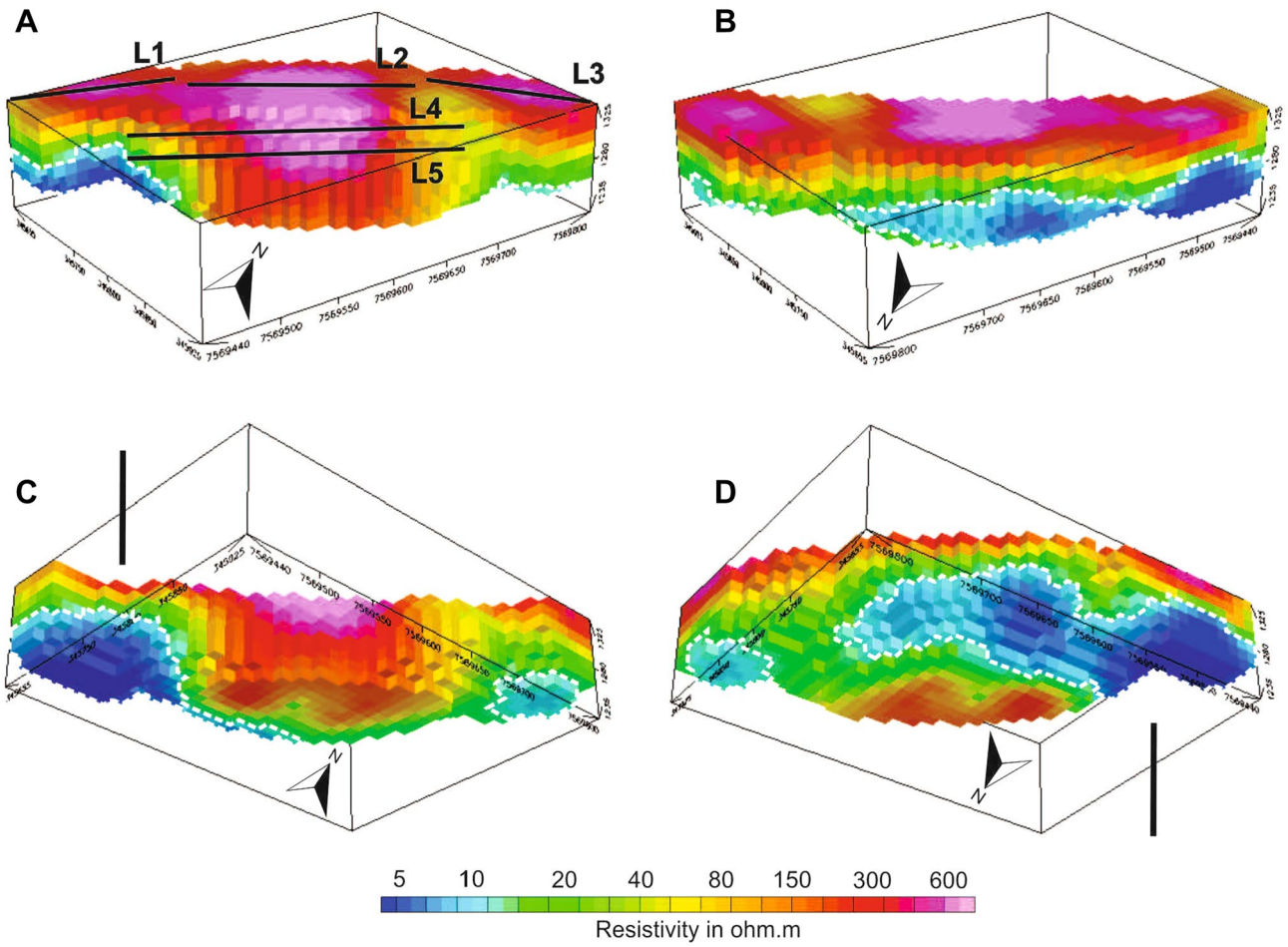

Fig. 6 Model of 3D blocks of electrical tomography: **a** front view; **b** back view; **c** base view; and **d** rear base view

that decreases with depth. This may be due to the presence of wet and clayey areas.

In the view of the front and rear base (Fig. 6c and d), a 9 Ωm point is also observed, indicating the presence of water on this side of the dam. However, according to the elevation, this water is inside the rock massif, below the dam. This flow is probably related to the low resistivities located in the upper sections due to the phenomenon of capillarity; this aspect was analyzed through the multilevel map model generated by the 3D interpolation model (Fig. 7), in which a more detailed model of the dam was produced, where layers of resistivity were selected every 10 m of depth, in order to study the interior of the dam.

In the multilevel map model, the curved line indicates the location of the horizontal drainage mat, which follows the structure's design; the vertical lines represent the lateral limit of the dike and the predominance of the rock massif at the ends of the model.

According to Fig. 7d, the dam has zones of low resistivity that indicate the presence of water at four relevant points, two of which are located inside the dam. However, the function of the drainage mat is to retain the flow of percolated water through the dam and the foundation, and prevent water from passing through the dam body. Figure 7d and e show that the water flow is blocked midway, exactly where the drainage mat is located, demonstrating that the system is functioning properly.

As previously mentioned, the right side of the dam has a less resistive region in the upper sections of the dam, with values up to 20 Ωm in the front region of the drainage mat, as highlighted in Fig. 7b; this increases with depth (Fig. 7c and g). In Fig. 7e, f and a second region is also indicated, which has resistivity values of 6–10 Ωm, indicating the presence of water. An analysis of Fig. 7f and g indicates that the water flows laterally, descending from NE to SW.

The least resistive section (5–9 Ωm) is on the left side of the dam, where there is a significant volume of water. Figure 7d and e show three low resistivity locations in the central and left side, and a significant increase in depth in the NW to SE direction. The presence of such anomalies,

interpreted as hydrogeological flows that occur at the base of the dam and inside the rock massif, suggest the following hypothetical origins:

- According to Oliveira and Brito (1998), a rock mass constitutes a heterogeneous system, essentially composed of localized discontinuities and defined by fractures. The water inside the rock massif, below and on the sides of the dam, is presumably flowing through these discontinuities that favor these fracture zones;
- Geophysical records show local and vertical low resistivity zones on the right side of the dam in the upper sections and deeper in the central and left side. This may be due to capillary flow. However, there is no evidence that these pose a risk to the physical integrity of the dam, because in the geophysical image sequence, it is possible to verify that the internal drainage system of the dam works well, draining the water from the structure as soon as the water reaches the chimney sub-vertical filter, and drainage mat.

Conclusions

The use of the ERT technique allowed us to identify flow zones within the rock massif below the dam. The combination of measurements and data modeling allows a clear diagnosis of flows within the rock massif, related to rock outcrops at the front base of the dam. In addition, 3D geophysical modeling was useful for identifying infiltration zones, researching piping áreas, and predicting failures. In addition, it is an important way to perform environmental diagnosis for the control, monitoring and early assessment of emerging dams.

The ERT lines showed high resistivity (600 Ωm) in portions of the upper sections, associated with the low humidity soil, and low resistivity (5 Ωm) zones that indicate the presence of wet areas on the sides of the dam, outside the drainage mat, which shows that the drainage system is functioning adequately.

This research found no evidence of internal erosion inside the dam, which reduces the risk of dam failure due to this factor; however, there are moist areas that could indicate the beginning of the erosion process. Areas of capillary flow are normal elements in an earth and rock dam and do not point to apparent risks to its physical integrity. Furthermore, it was possible to verify the efficiency of the internal drainage system – chimney sub-vertical filter + drainage mat (Fig. 7). The dam spillway, a tulip-like structure, was the biggest risk factor. However, a new surface flow system was built in May 2019, and the old one was isolated.

The 3D interpolation blocks made it possible to recognize the flow paths within the rock massif below the dam. On the left side of the structure, a larger volume of water was found, which flows from NW to SE, which indicated flow within the rock massif through fracture zones that emerge at the front base of the dam. This was confirmed to align with the orientation of the fracture plane N40W/38SW, studied in the water upwelling zone.

As for the upwelling area, chemical analysis of the local water is recommended to establish its possible relationship with the water in the dam, in addition to the planning of a waterproofing system based on the structural pattern and geophysical results.

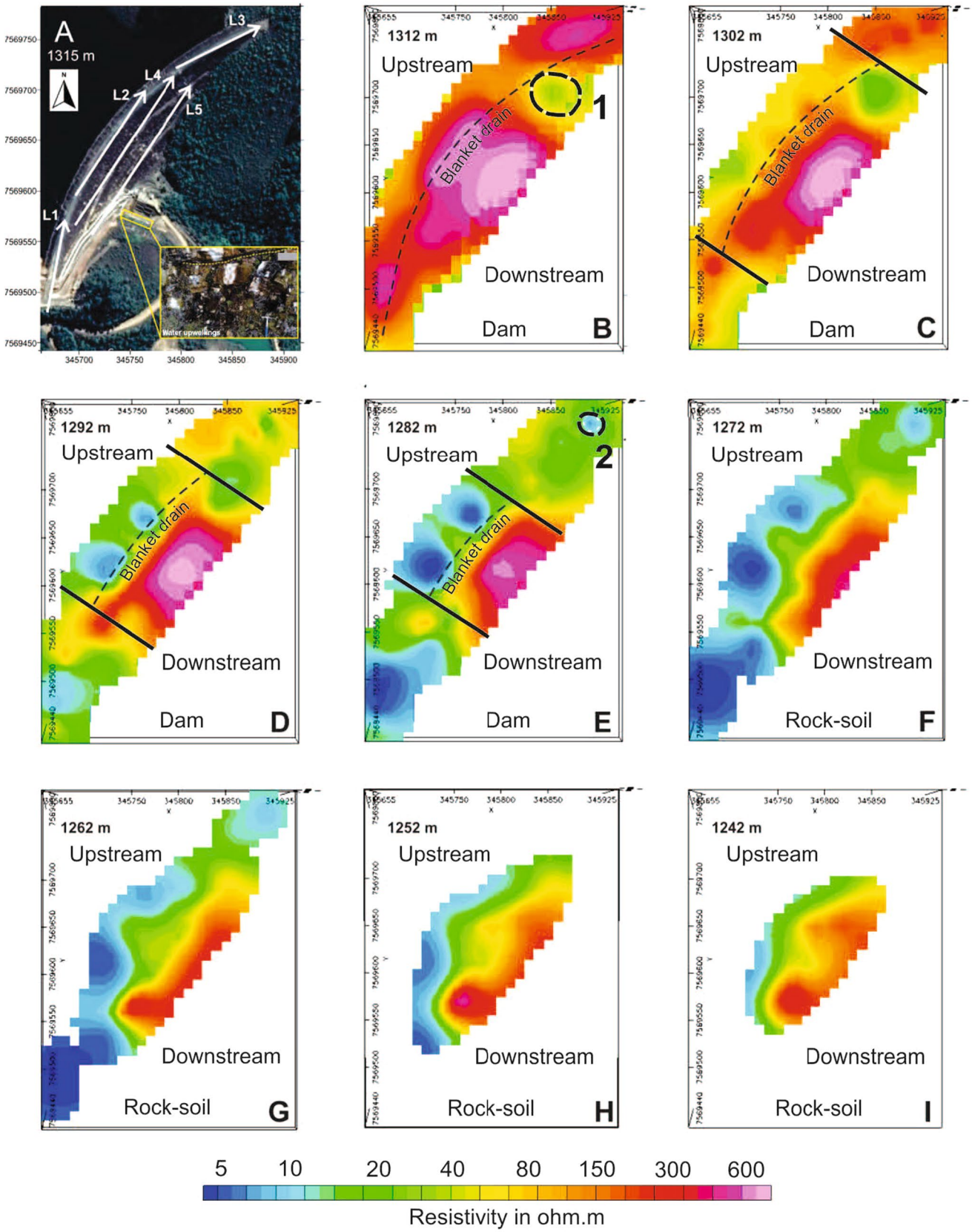
A
1315 m
L1
L2
L3
L4
L5
Water upwellings
1312 m
Upstream
Blanket drain
1
Downstream
Dam
B
1302 m
Upstream
Blanket drain
Downstream
Dam
C
1292 m
Upstream
Blanket drain
Downstream
Dam
D
1282 m
Upstream
2
Blanket drain
Downstream
Dam
E
1272 m
Upstream
Downstream
Rock-soil
F
1262 m
Upstream
Downstream
Rock-soil
G
1252 m
Upstream
Downstream
Rock-soil
H
1242 m
Upstream
Downstream
Rock-soil
I
5 10 20 40 80 150 300 600
Resistivity in ohm.m

◂**Fig. 7** 3D interpolation model, with 10 m depth increments: **a** Arrangement of geophysical lines in the study area; **b** 3D interpolation model at 1312 m; **c** 3D interpolation model at 1302 m; **d** 3D interpolation model at 1292 m; **e** 3D interpolation model at 1282 m; **f** 3D interpolation model at 1272 m; **g** 3D interpolation model at 1262 m; **h** 3d interpolation model at 1252 m; **i** 3D interpolation model at 1242 m

Acknowledgements The authors thank the Foundation for Research Support of the State of Sao Paulo (Fundação de Amparo a Pesquisa do Estado de São Paulo—FAPESP process No. 2018 / 14565-3) and the INB for the support.

References

ABEM (2012) Terrameter LS—instruction manual. Sundbyberb, Sweden

Albuquerque R, Braga MA, Andrade-Oliveira L, Santana de Oliveira-Dias L, Pinto-Almeida LA, Oliveira AH, Brandão S (2019) Caracterização de barragens de rejeito usando geofísica rasa: aplicação na Barragem B1 de Cajati, São Paulo. Anuário do Instituto de Geociências. https://doi.org/10.11137/2019_1_567_579 **[in Portuguese]**

Al-Fares W (2014) Application of electrical resistivity tomography technique for characterizing leakage problem in Abu Baara earth dam, Syria. Geophys J Int. doi.https://doi.org/10.1155/2014/368128

Asfahani J, Radwan Y, Layyous I (2010) Integrated geophysical and morphotectonic survey of the impact of Ghab extensional tectonics on the Qastoon dam, northwestern Syria. Pure Appl Geophys 167:323–338

Assumpção M, Marza V, Barros L, Chimpliganond C, Soares J, Carvalho J, Caixeta D, Amorim A, Cabral E (2002) Reservoir-induced seismicity in Brazil. Pure Appl Geophys 159:597–617

Bedrosian PA, Burton BL, Powers MH, Minsley BJ (2012) Geophysical investigations of geology and structure at the Mathis Creek Dam, Truckee, California. J Appl Geophys 77:7–20

Bièvre G, Lacroix P, Oxarango L, Goutaland D, Monnot G, Fargier Y (2017) Integration of geotechnical and geophysical techniques for the characterization of a small earth-filled canal dyke and the localization of water leakage. J Appl Geophys 139:1–15. https://doi.org/10.1016/j.jappgeo.2017.02.002

Camarero P, Moreira CA, Garcia H (2019) Analysis of the physical integrity of earth dams from electrical resistivity tomography (ERT) in Brazil. Pure Appl Geophys 176:5363–5375. https://doi.org/10.1007/s00024-019-02271-8

Chandler RJ, Tosatti G (1995) The Stava tailings dams failure, Italy, July 1985. Proc Inst Civ Eng Geotech Eng 113:67–79

Coulibaly Y, Belem T, Cheng L (2017) Numerical analysis and geophysical monitoring for stability assessment of the northwest tailings dam at Westwood Mine. Int J Min Sci Technol 27:701–710. https://doi.org/10.1016/j.ijmst.2017.05.012

Franklin MR (2007) Modelagem numerica do escoamento hidrológico e dos processos geoquímicos aplicados à previsão da drenagem ácida em uma pilha de estéril da mina de urânio de Paço de Caldas-MG. PhD Diss, Univ Federal of Rio de Janeiro **[in Portuguese]**

IBAMA (2017) Apresenta informaçoes em O que e segurança de barragens. IBAMA, Brasília, Brazil. www.ibama.gov.br/emergencias-ambientais/seguranca-de-barragens/o-que-e-seguranca-de-barragens. Acessed 10 Mar 2018 **[in Portuguese]**

IBAMA (2019) Apresenta Rompimento de barragem da Vale em Brumadinho (MG) destruiu 269,84 hectares. IBAMA, Brasília, Brazil. www.ibama.gov.br/noticias/730-2019/1881-rompimento-de-barragem-da-vale-em-brumadinho-mg-destruiu-269-84-hectares. Acessed 15 Apr 2019 **[in Portuguese]**

Kearey P, Brooks M, Hill I (2002) An introduction to geophysical exploration. Wiley-Blackwall Science, New York

Knödel K, Lange G, Voigt HJ (2007) Enviromental geology—handbook of fields methods and case studies. Springer, Berlin

Lewis B (2014) Small dams: planning, construction and maintenance. CRC Press, Melbourne

Lghoul M, Teixidó T, Peña JA, Hakkou R, Kchikach A, Guérin R, Jaffal M, Zouhri L (2012) Electrical and seismic tomography used to image the structure of a tailings pond at the abandoned Kettara Mine, Morocco. Mine Water Environ 31:53–61. https://doi.org/10.1007/s10230-012-0172-x

Lin CP, Hung YC, Yu ZH, Wu PL (2013) Investigation of abnormal seepages in an earth dam using resistivity tomography. J Geol Eng 8:61–70

Lin CH, Lin CP, Hung YC, Chung CC, Wu PL, Liu HC (2018) Application of geophysical methods in a dam project: life cycle perspective and Taiwan experience. J Appl Geophys. https://doi.org/10.1016/j.jappgeo.2018.07.012

Loke MH (2000) Electrical imaging surveys for environmental and engineering studies. A practical guide to 2-D and 3-D surveys

Lowrie W (2007) Fundamentals of geophysics, 2nd edn. Cambridge University Press, New York City

Mainali G (2006) Monitoring of tailings dams with geophysical methods. Thesis, Luleå University of Technology

Minsley BJ, Burton BL, Ikard S, Powers MH (2011) Geophysical investigations at Hidden Dam, Raymond, California: Summary of fieldwork and data analysis. USGS Open File Report 2010–2013. https://pubs.er.usgs.gov/publication/ofr20101013

Moreira CA, Gonçalves LC, Lopes TC, Melo LI (2017) DC resistivity investigation in a fractured aquifer system contaminated by leachate from an old dump. Geofis Int 56:345–358

Mussett AE, Khan MA (2000) Looking into the earth: an introduction to geological geophysics. Cambridge University Press, New York City

Oh S, Sun CG (2007) Combined analysis of electrical resistivity and geotechnical SPT blow counts for the safety assessment of fill dam. Environ Geol 54:31–42

Oliveira AMS, Brito SNA (1998) Geologia de engenharia. ABGE Press, São Paulo (**[in Portuguese]**)

Osazuwa IB, Chinedu AD (2008) Seismic refraction tomography imaging of high-permeability zones beneath an earthen dam, in Zaria area, Nigeria. J Appl Geophys 66:44–58

Ozcan NT, Ulusay R, Isik NS (2013) A study on a geotechnical characterization and stability of downstream slope of a tailings dam to improve its storage capacity (Turkey). Environ Earth Sci 69:1871–1890

Sammarco OA (2004) Tragic disaster caused by the failure of tailings dams leads to the formation of the Stava 1985 foundation. Mine Water Environ 23:91–95. https://doi.org/10.1007/s10230-004-0045-z

Sentenac P, Benes V, Keenan H (2018) Reservoir assessment using non-invasive geophysical techniques. Environ Earth Sci 77:293. https://doi.org/10.1007/s12665-018-7463-x

Sjödahl P, Dahlin T, Johansson S (2005) Using resistivity measurements for dam safety evaluation at Enemossen tailings dam in southern Sweden. Environ Geol 49:267–273. https://doi.org/10.1007/s00254-005-0084-1

Thompson S, Kulessa B, Luckman A (2012) Integrated electrical resistivity tomography (ERT) and self-potential (SP) techniques for assessing hydrological processes within glacial lake moraine dams. J Glaciol 58:849–858. https://doi.org/10.3189/2012JoG11J235

Waber N, Schorscher HD, Peters T (1992) Hydrothermal and supergene uranium mineralization at the Osamu Utsumi mine, Poços de Caldas, Minas Gerais, Brazil. J Geochem Explor 45:53–112

Wei Z, Yin G, Wan L, Li G (2016) A case study on a geotechnical investigation of drainage methods for hightening a tailing dam. Environ Earth Sci 75:106. https://doi.org/10.1007/s12665-015-5029-8

World Nuclear Association (2020) World Nuclear Performance Report 2020. www.world-nuclear.org/information-library/current-and-future-generation/plans-for-new-reactors-worldwide.aspx Acessed 19 Jun 2020

Zarroca M, Linares R, López PCV, Roqué C, Rodríguez R (2014) Application of electrical resistivity imaging (ERI) to a tailings dam project for artisanal and small-scale gold mining in Zaruma-Portovelo, Ecuador. J Appl Geophys 113:103–113. https://doi.org/10.1016/j.jappgeo.2014.11.022